Tailoring sodium accessibility in RuCu-Na_2ZrO_3 catalyst for tunable CO_2 hydrogenation pathways.

Introduction

Rising atmospheric CO_2 concentrations driven by anthropogenic activities pose a significant threat to global climate stability, necessitating urgent mitigation strategies. Among available approaches, catalytic CO_2 hydrogenation is particularly attractive as it integrates CO_2 utilisation with renewable H_2 (Anwar et al., 2020). While methane has traditionally been targeted, increasing attention is shifting toward CO due to its role as a key syngas intermediate and versatile feedstock for downstream synthesis (Hu et al., 2024; Ye et al., 2025). However, CO_2-to-CO conversion via the reverse water-gas shift (RWGS) reaction is thermodynamically favoured at elevated temperatures (T> 600 °C), resulting in high-energy demands and catalyst sintering. Consequently, the development of catalysts capable of operating efficiently at lower temperatures is critical.

Ruthenium exhibits high activity and excellent H_2 dissociation ability while copper offers favourable CO selectivity and cost advantages though prone to sintering at high temperature (Choi et al., 2024; Rabelo-Neto et al., 2022). Lots of studies show that alkali promotion, particularly with sodium, enhances surface basicity and facilitates formate intermediates, promoting CO formation while suppressing methanation (Liao et al., 2025; Seuser et al., 2023; Xu et al., 2021). Despite this, the influence of sodium distribution which is governed by synthesis route and its synergy with the support and metal site, remains unexplored. This study investigates its impact on CO_2 conversion and product selectivity.

Method

2.1 Catalyst preparation

Na_2CO_3, ZrO_2, $RuCl_3.xH_2O$, and $CuCl_2.2H_2O$ (≥ 99.9 %, Sigma Aldrich) were used as received. Catalysts (2 wt% Ru, 4wt % Cu) were synthesised via wet impregnation to isolate the effect of Na distribution. Method A **(**RuCu - Na_2ZrO_3-A): precursors were dissolved in 20 mL H2O, stirred (40 °C, 480 rpm, 2 hr), dried (60 °C, overnight), ground, and calcined (720 °C for 10 h, 1 °C /min). Method B **(**RuCu - Na_2ZrO_3-B): As method A followed by filtration prior to drying to obtain a Na-depleted sample. Method C **(**RuCu - Na_2ZrO_3-C):As method A, using pre-synthesized Na_2ZrO_3 (Munro et al., 2020).

2.2 Catalyst characterization

X-Ray Diffraction (XRD) patterns were collected over 2θ range of 5-85 °C using a Bruker Nonius X8-Apex2 CCD diffractometer. Surface composition was analysed by X-ray Photoelectric Spectroscopy (XPS, AI Kα, 1486.6 eV) under ultra-high vacuum (<$1x10^{-9}$ mbar).

2.5 Catalytic Activity Tests

Reactions were conducted in a fixed-bed quartz reactor (30 mg of catalyst diluted with quartz sand). Experiments were performed at 240 °C and 400 °C (10 °C/min) under H_2/CO_2 flow of 3:1, with effluent gases analysed using a gasboard-3100 analyser.
Blank tests were performed and subtracted. All experiments were conducted in triplicate with error being <12%.
CO_2 conversion, selectivity, and yield were calculated as:

$$X_{CO2} = \frac{nCO2\ adsorbed - nCO2\ product}{nCO2\ adsorbed} \times 100$$

$$S_{CO/CH4} = \frac{nCO/CH4\ out}{nCO2\ converted} \times 100$$

$$Y_{CO/CH4} = \frac{nCO/CH4\ out}{nCO2\ adsorbed} \times 100$$

Results and discussion

Figure 1 shows the x-ray diffraction patterns of catalysts, all of which exhibit crystalline phases of ZrO_2, Na_2ZrO_3, Ru-metal, RuO_2, Na_2CO_3 and CuO. The diffractograms confirm monoclinic Na_2ZrO_3 as the primary crystalline phase. (2θ = 18.2° and 33.8°) across all samples. Catalyst C additionally shows a weak Na_2CO_3 peak at 30.4°, likely originating from unreacted synthesis residue. Catalyst B shows a prominent peak at 18.2 ° indicative of <50 % Na^+ site occupancy of the Na layer because of the Na depletion during synthesis. It also displayed distinct peaks corresponding to both metallic Ru0 (42.4°, 44.7° and 59.4°) and RuO_2 (55.4°), a combination known to enhance CO_2 hydrogenation activity (Chang et al., 2024). In contrast, Catalyst A and C only showed weak reflections of RuO_2. Overall, the XRD patterns show that Ru and its oxide exist as separate crystalline phases rather than being incorporated into the sodium Zirconate lattice.

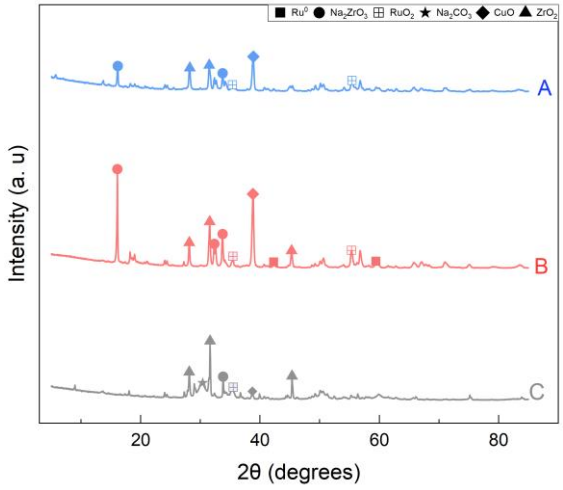

Figure 1 *Diffraction patterns for A) RuCu-Na_2ZrO_3-A; B) RuCu-Na_2ZrO_3-B; C) RuCu-Na_2ZrO_3-C*

XPS analysis (Table 1) revealed that the surface Ru and Cu contents were significantly lower than their nominal loadings, with Ru near 1 at% and Cu ranging from 0.4- 1.53 at.%. The Na-depleted RuCu-Na_2ZrO_3-B showed 40% less Na than the other Na-containing samples, confirming its synthesis route and aligning with XRD results (Figure 1). Notably, Na depletion increased the Ru:Cu surface ratio, indicating reduced site blocking and improved formation of Cu-Zr interfacial sites

Table 1: Atomic concentrations (%) showing dispersion of metals for RuCu-Na_2ZrO_3-A, -B, -C.

Catalyst	Na 1s (%)	Cu 2p (%)	O 1s (%)	Ru 3p (%)	Zr 3p (%)	C 1s (%)
RuCu -Na_2ZrO_3 -A	16.9	0.39 Cu (II)	45.54	1.12 Ru (IV)	6.27 Zr (IV)	29.84
RuCu -Na_2ZrO_3 -B	7.2	1.53	52.21	1.07	16.2	20.39
RuCu -Na_2ZrO_3 -C	21.6	0.42 Cu (II)	45.42	0.91 Ru (IV)	3.45 Zr (IV)	27.48

Results of catalytic reaction are presented in Figure 2, with CH_4 and CO as the primary products. At 400 °C (Figure 2a) clear differences are observed among the catalysts. RuCu-Na_2ZrO_3-B shows the highest activity, achieving superior CO yield (44.7 $mmolg^{-1}h^{-1}$), CO_2 conversion (31.3 %), and CH_4 yield (6.9 $mmolg^{-1}$ h^{-1}). This indicates effective promotion of both RWGS and subsequent methanation. The enhanced performance is attributed to optimised sodium distribution, where partial

Na removal reduces site blocking while maintaining sufficient basicity for CO_2 adsorption, consistent with reports of decreased conversion at higher Na loadings (Seuser et al., 2023). In contrast, RuCu-Na_2ZrO_3-A and RuCu-Na_2ZrO_3-C exhibit lower activity due to less favourable Na configurations, which limit active site accessibility and hydrogenation (Sanna et al., 2025).

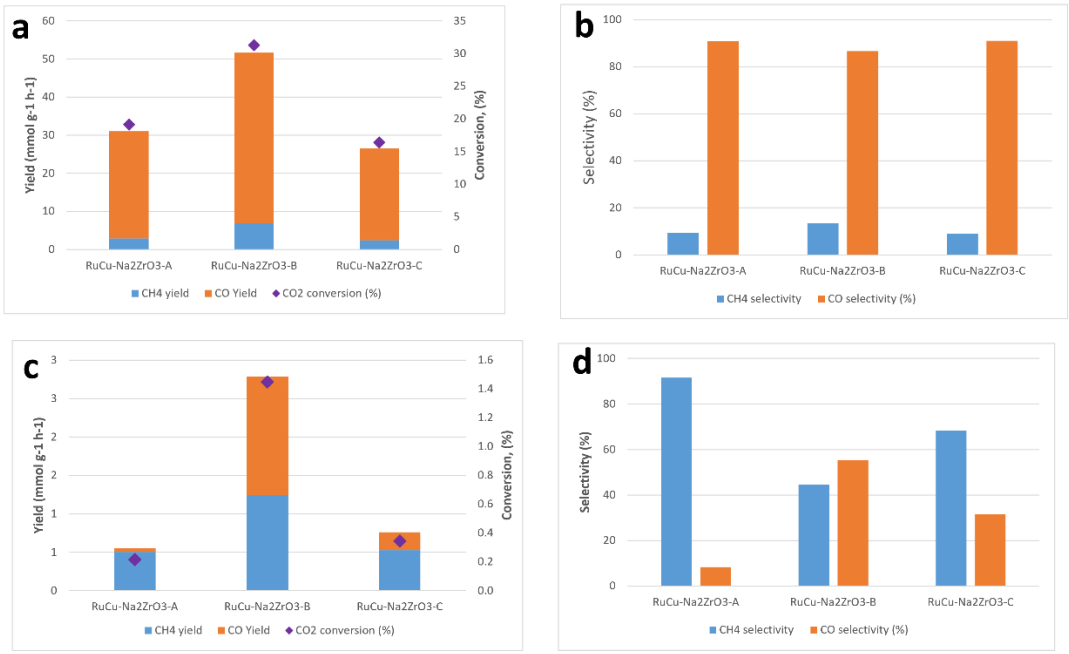

Figure 2 *a): CO_2 conversion and product yields (CO, CH_4) at 400 °C b) product selectivity at 400 °C; c): CO_2 conversion and yields over at 240 °C; d) product selectivity trends at 240 °C for RuCu-Na_2ZrO_3-A,B,C*

Figure 2b presents the selectivity profiles at 400 °C, complimenting the activity trends. All catalysts show high CO selectivity (86-91 %), and low CH_4 selectivity, confirming RWGS dominance, which can be linked to Cu-assisted CO desorption and moderated hydrogenation pathways (Choi et al., 2024).
In Fig 2c & d, the performance at 240 °C are reported, the activity trend remains unchanged when comparing the three materials with results obtained at 400 °C, but conversions are consistently lower. Another key difference is that selectivity on CH_4 increases for all three materials, however, only RuCu-Na_2ZrO_3-B could maintain a relatively high CO selectivity (55.4 %) at 240 °C where methanation is thermodynamically favoured. Overall, RuCu-Na_2ZrO_3-B achieves the best balance between RWGS and methanation, while RuCu-Na_2ZrO_3-A and -C prioritise selectivity at the expense of activity.

Conclusion

This work set out to investigate the effect of sodium distribution, which is controlled via synthesis route, on the performance of RuCu-Na_2ZrO_3 catalysts for CO_2 hydrogenation. The results demonstrate that tailoring sodium accessibility, rather than simply its loading, is critical to catalyst design. The filtration-modified synthesis (RuCu-Na_2ZrO_3-B) produced a more favourable sodium environment that minimised site blocking while preserving sufficient basicity, thereby enabling enhanced CO_2 activation and improved utilisation of active Ru and Cu sites. This led to superior catalytic performance (31.3% conversion, 44.7 mmol g^{-1} h^{-1} CO yield, and 6.9 mmol g^{-1} h^{-1} CH_4 yield) at 400 °C and even under low-temperature conditions (240 °C) where CO_2 activation is limited. In contrast, excess or structurally constrained sodium in RuCu-Na_2ZrO_3- A and -C limited active site accessibility, reducing overall efficiency. The observed activity-selectivity trade-off further confirmed that sodium distribution governs the balance between competing RWGS and methanation pathways. This study

establishes synthesis-controlled sodium distribution as a key lever for tuning Ru-Cu supported catalyst performance, providing a practical strategy for designing efficient systems for CO_2 utilisation.

Acknowledgements

The authors gratefully acknowledge the Nigerian Petroleum Technology Development Fund (PTDF) for the PhD sponsorship and financial support that enabled this research (Grant No. POSS2022000000049782

References

Anwar, M. N., Fayyaz, A., Sohail, N. F., Khokhar, M. F., Baqar, M., Yasar, A., Rasool, K., Nazir, A., Raja, M. U. F., Rehan, M., Aghbashlo, M., Tabatabaei, M., & Nizami, A. S. (2020). CO(2) utilization: Turning greenhouse gas into fuels and valuable products. *Journal of Environmental Management*, *260*, 110059. https://doi.org/10.1016/j.jenvman.2019.110059

Chang, R., Menon, A. S., Svensson Grape, E., Broqvist, P., Inge, A. K., & Cheung, O. (2024). Rethinking the existence of hexagonal sodium zirconate CO2 sorbent. *Journal of Materials Chemistry A*, *12*(26), 15858–15865. https://doi.org/10.1039/d4ta01681e

Choi, Y., Sim, G. D., Jung, U., Park, Y., Youn, M. H., Chun, D. H., Rhim, G. B., Kim, K. Y., & Koo, K. Y. (2024). Copper catalysts for CO2 hydrogenation to CO through reverse water–gas shift reaction for e-fuel production: Fundamentals, recent advances, and prospects. *Chemical Engineering Journal*, *492*. https://doi.org/10.1016/j.cej.2024.152283

Hu, J., Cai, Y., Xie, J., Hou, D., Yu, L., & Deng, D. (2024). Selectivity control in CO2 hydrogenation to one-carbon products. *Chem*, *10*(4), 1084–1117. https://doi.org/10.1016/j.chempr.2024.02.017

Liao, W., Nguyen, A., & Liu, P. (2025). Alkali-induced catalytic tuning at metal and metal oxide interfaces. *Chem Soc Rev*, *54*(9), 4164–4182. https://doi.org/10.1039/d4cs01094a

Munro, S., Åhlén, M., Cheung, O., & Sanna, A. (2020). Tuning Na2ZrO3 for fast and stable CO2 adsorption by solid state synthesis. *Chemical Engineering Journal*, *388*. https://doi.org/10.1016/j.cej.2020.124284

Rabelo-Neto, R. C., Almeida, M. P., Silveira, E. B., Ayala, M., Watson, C. D., Villarreal, J., Cronauer, D. C., Kropf, A. J., Martinelli, M., Noronha, F. B., & Jacobs, G. (2022). CO2 hydrogenation: Selectivity control of CO versus CH4 achieved using Na doping over Ru/m-ZrO2 at low pressure. *Applied Catalysis B: Environmental*, *315*. https://doi.org/10.1016/j.apcatb.2022.121533

Sanna, A., Reddy, K. P., Emehel, C., Bagnato, G., Barba-Nieto, I., Bos, J. W., & Rodriguez, J. A. (2025). Integrated CO2 capture and hydrogenation in presence of Ru–Na2ZrO3: An in-situ study. *International Journal of Hydrogen Energy*, *121*, 118–131. https://doi.org/10.1016/j.ijhydene.2025.03.341

Seuser, G., Staffel, R., Hocaoglu, Y., Upton, G. F., Garcia, E. S., Cronauer, D. C., Kropf, A. J., Martinelli, M., & Jacobs, G. (2023). CO(2) Hydrogenation: Na Doping Promotes CO and Hydrocarbon Formation over Ru/m-ZrO(2) at Elevated Pressures in Gas Phase Media. *Nanomaterials (Basel)*, *13*(7). https://doi.org/10.3390/nano13071155

Xu, J., Gong, X., Hu, R., Liu, Z.-w., & Liu, Z.-t. (2021). Highly active K-promoted Cu/β-Mo2C catalysts for reverse water gas shift reaction: Effect of potassium. *Molecular Catalysis*, *516*. https://doi.org/10.1016/j.mcat.2021.111954

Ye, R., Ding, J., Reina, T. R., Duyar, M. S., Li, H., Luo, W., Zhang, R., Fan, M., Feng, G., Sun, J., & Liu, J. (2025). Design of catalysts for selective CO2 hydrogenation. *Nature Synthesis*, *4*(3), 288–302. https://doi.org/10.1038/s44160-025-00747-1